IEEE Access
Multidisciplinary ⋮ Rapid Review ⋮ Open Access Journal

Received October 9, 2018, accepted November 1, 2018, date of publication December 12, 2018,
date of current version December 31, 2018.

Digital Object Identifier 10.1109/ACCESS.2018.2883353

Fabrication and Characterization of Capacitive RF MEMS Perforated Switch

K. SRINIVASA RAO[1], (Member, IEEE), LAKSHMI NARAYANA THALLURI[1,2], (Member, IEEE), KOUSHIK GUHA[3], AND K. GIRIJA SRAVANI[1,3]

[1]MEMS Research Center, Department of Electronics & Communication Engineering, Koneru Lakshmaih Education Foundation (Deemed to be University), Guntur 522502, India
[2]Dr. A. P. J. Abdul Kalam Research Forum, Department of Electronics and Communication Engineering, Andhra Loyola Institute of Engineering and Technology, Vijayawada 520008, India
[3]National MEMS Design Center, Department of Electronics and Communication Engineering, National Institute of Technology at Silchar, Silchar 788010, India

Corresponding author: K. Srinivasa Rao (srinivasakarumuri@gmail.com)

This work, Fabrication of the Device was supported by CeNSE, Indian Institute of Science, Bengaluru, through the Ministry of Electronics and Information Technology (MeitY), Govt. of India.

ABSTRACT In this paper, we have designed, simulated, fabricated, and characterized a clamped-clamped micro mechanical structure-based shunt capacitive RF MEMS switch. The clamped–clamped micromechanical structure is micromachined using a gold metal thickness of 500 nm. AlN is used as a dielectric material, and it is deposited using the dc sputtering PVD process. In the MEMS technology, particularly in devices fabrication, releasing the membrane is a difficult task, and here, we have presented a novel wet process to release the membrane. Primarily, the S1813 sacrificial layer is etched by using the piranha solution and cleaned with the IPA solution. Critical point drying is done after fabrication to reduce the stiction effect on the switch. Overall, the switch requires the pull-in voltage of 5.5 V for 1.8-μm displacement. In the process of optimization, primarily, the switch is designed and simulated using finite-element method tools. The reliability of the capacitive RF MEMS switches depends on the stiction problem caused by dielectric charging, and the proposed capacitive switch dielectric charging behavior is characterized using the CV curve method.

INDEX TERMS CPW transmission line, MEMS Technology, micromachining, metal and dielectric material deposition, MEMS structure release, dielectric charging.

I. INTRODUCTION

Last few decades, MEMS technology based communication devices like filters, switches, phase shifters and antennas are showing significant domination when compared with traditional Solid State Technology (CMOS and FET) devices. The present and future communication applications like cognitive radios and *ad hoc* networks require low loss reconfigurable antennas with enhanced features in terms of frequency and polarization. RF MEMS switches are showing great potential in terms of low loss and high isolation to design reconfigurable antennas at microwave range [1]–[4].

Prior to fabrication, design and simulation are the basic concerns in the process of RF MEMS switch optimization in terms of dimensions and materials. At design and simulation level of RF MEMS switches, reducing the pull-in voltage, increasing the isolation, analysis of stiffness of the membrane to avoid buckling and to improve the reliability, easing the actuation process, selection of thin films are the major research issues. Low pull-in voltage and low power consumption of RF MEMS switches improves the battery backup of the communication devices. The low pull-in voltage enables the interface of MEMS devices with integrated circuits. If the switch is offering high isolation we can avoid the RF leakages in reconfigurable devices [5]–[15].

Buckling and stiction are the two major challenging issues in fabrication process which are influencing the reliability factor of RF MEMS switch [16]–[26]. Since the RF performance of the switch depends on the bridge height, the buckling or stiction is an undesired effect. Critical point drying (CPD) helps to avoid the stiction failures caused by dielectric charging [27]–[29]. Few methods like pull-in voltage finding and CV curve shifting are popular to characterize the dielectric charging behavior of the capacitive RF MEMS switches [30]–[35]. The main objective of this paper is fabrication low pull-in voltage and high isolation offering minimum stiction shunt capacitive RF MEMS switch.

In this study, one of the research challenges like reducing actuation voltage, increasing the isolation and fabrication issues like buckling and stiction problems are reported and analyzed. The paper is organized as follows: in Section II, we holistically investigate the mechanical and microwave parameters like pull-in voltage, resonant frequency, spring constant, insertion and isolation losses. Section III describes the design considerations for low pull-in voltage, high isolation buckling free RF MEMS switch. Lastly, the measurement results for the fabricated stiction free switch is presented and discussed in Section IV and followed by Conclusions in Section V.

II. SWITCH PARAMETRIC MODELLING

In this paper, we have designed and fabricated an electrostatically actuated, vertical deflective clamped-clamped membrane based shunt capacitive RF MEMS switch. The micro mechanical RF switches modeling involves the mechanical and radio frequency analysis parameters.

A. PULL-IN VOLTAGE

In the investigation, we noticed that the electrostatically actuated switch pull-in voltage depends on spring constant of the micro mechanical structure. In capacitive RF MEMS switch, one plate is fixed one and the other plate is movable as shown in Figure 1. The electrostatic actuation in the RF MEMS switches is because of the electrostatic force created by voltage applied between the electrodes i.e., top membrane and bottom electrode.

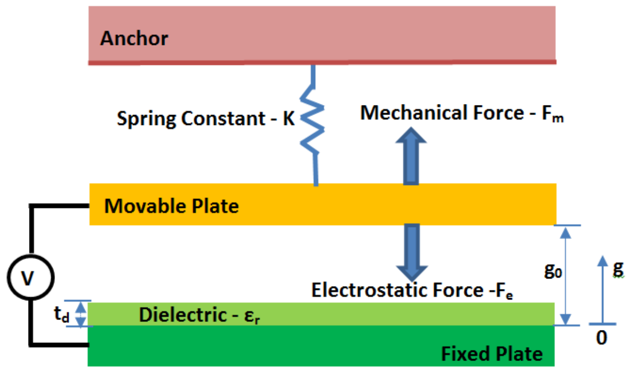

FIGURE 1. **Electrostatic actuation in RF MEMS switches.**

In electrostatic actuation, two forces are influence the movable plate, one is electrostatic force (F_e) and other one is mechanical restoration force (F_m). The mechanical restoration force is equal to the rate of change of potential energy w.r.t. displacement ((g_0-g)=δ) i.e., [36]

$$F_m = \frac{dE_p}{d(g_0 - g)} = k(g_0 - g) = K\delta \tag{1}$$

where,

Elastic potential energy $= E_p = \frac{1}{2}K(g_0 - g)^2 = \frac{1}{2}K\delta^2$.

When we apply a voltage 'V' between the two parallel plates, then an electrostatic energy generates between parallel plates. The generated electrostatic energy can be written as

$$\text{Electrical energy} = E_e = \frac{1}{2}CV^2 \tag{2}$$

In the RF MEMS switch capacitor plates, one plate is movable and other one is fixed then the electrostatic force in the variable capacitor is

$$\text{Electrostatic force} = F_e = \frac{1}{2}V^2\frac{dC(g)}{dg} = -\frac{\varepsilon_0 AV^2}{2g^2} \tag{3}$$

Under equilibrium condition; electrostatic force (F_e) and the mechanical restoration force (F_m) are equal i.e.,

$$\begin{aligned} F_e &= F_m \\ \frac{1}{2}\frac{\varepsilon_0 AV^2}{g^2} &= K(g_0 - g) \\ \text{Supply voltage} = V &= \sqrt{\frac{2K}{\varepsilon_0 A}g^2(g_0 - g)} \end{aligned} \tag{4}$$

When the supply voltage is equal or greater than the pull-in voltage, the electrostatic force dominates the mechanical force associated with the membrane, and then the membrane will collapse. Apply the derivative to supply voltage w.r.t height of the movable plate (g), and equate to zero i.e.,

$$\begin{aligned} \frac{dV}{dg} &= 0 \\ \frac{2K}{\varepsilon_0 A}2gg_0 - \frac{2K}{\varepsilon_0 A}3\varepsilon^2 &= 0 \\ g &= \frac{2g_0}{3} \end{aligned} \tag{5}$$

The above relation states that, at 2/3 of gap the structure loose its stability and it will collapse, i.e., if the structure reaches to 2/3 gap for applied supply voltage then the electrostatic force will dominate the mechanical force. Therefore, by substitute the "g" value in supply voltage (eq. 4), we will get the expression for pill-in voltage i.e.

$$V_{pull\_in} = V|_{g=\frac{2g_0}{3}} = \sqrt{\frac{8K}{27\varepsilon_0 A g_0^3}} \tag{6}$$

B. RESONANT FREQUENCY

The potential energy of a mechanical structure is often stored in springs and the kinetic energy is due to the motion of the mass. Both the energies in the electrostatic actuation can be written as,

$$\text{Potential energy}_{(\text{spring})} = \frac{1}{2}K\delta^2 \tag{7}$$

$$\text{Kinetic energy}_{(\text{mass})} = \frac{1}{2}m\dot{\delta}^2 \tag{8}$$

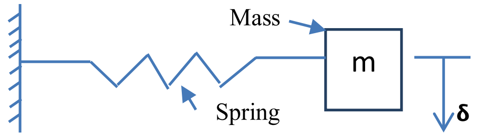

FIGURE 2. **Roof mass(m) with spring constant (K).**

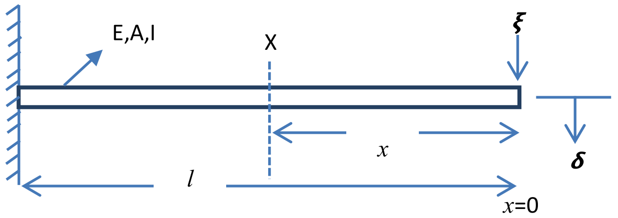

FIGURE 3. A cantilever beam with concentrated load (ξ) at the free end.

At two different time t_1 and t_2, the increase in potential energy must be equal to a decrease in kinetic energy (or visa versa)

$$(\text{Potential energy})_{\max} = (\text{Kinetic energy})_{\max} \tag{9}$$

Let us apply the signal $\delta(t)=A\,\mathrm{Sin}(\boldsymbol{\omega}_0 t+\boldsymbol{\phi})$ to the membrane, and equate the maximum potential and kinetic energies. This will help us to give the expression for resonant frequency of the membrane i.e.

$$\frac{1}{2}KA^2 = \frac{1}{2}m(\omega_0 A)^2$$

$$\text{Resonant frequency} = \omega_0 = \sqrt{\frac{K}{m}} \tag{10}$$

C. SPRING CONSTANT

From the simple bernoulli-euler and timoshenko beam bending theory, we can write the relation between bending stress (σ), bending momentum (M), moment of inertia (I), young's modules (E), radius of curvature (R), distance of fiber from natural axis (δ) i.e., [37]–[45]

$$\frac{\sigma}{\delta} = \frac{M}{I} = \frac{E}{R} \tag{11}$$

Therefore, the above expression represents the shear force, whereas the rate of intensity of loading can also be found out by differentiating the expression for shear force.

$$\text{Slope} = I_s = EI\frac{d\delta}{dx} \tag{12}$$

$$\text{Bending moment} = M = EI\frac{d^2\delta}{dx^2} \tag{13}$$

$$\text{Shear force} = F = EI\frac{d^3\delta}{dx^3} \tag{14}$$

$$\text{Load distribution} = \xi = EI\frac{d^4\delta}{dx^4} \tag{15}$$

The expression for deflection (δ) using differential equation is defined as

$$M = EI\frac{d^2\delta}{dx^2}$$

$$\frac{M}{EI} = \frac{d^2\delta}{dx^2}$$

Two times apply Integration on both sides i.e.

$$\delta = \int\int \frac{M}{EI}dx + Ax + B \tag{16}$$

where A & B are constants of integration to be evaluated from the known conditions of slope and deflections for the particular value of x. A cantilever beam is subjected to a concentrated load (**ξ**) at the free end, it is required to determine the deflection of the beam. In order to solve this problem, consider any x-section, x-x located at a distance x from the left end or the reference, and write down the expressions for the shear force and the bending moment,

$$F|_{x-x} = -\xi \tag{17}$$

$$M|_{x-x} = -\xi x \tag{18}$$

Substituting the value of M in terms of x then integrating the equation (13) then we will get i.e.

$$\frac{M}{EI} = \frac{d^2\delta}{dx^2}$$

$$\frac{-\xi x}{EI} = \frac{d^2\delta}{dx^2}$$

$$\frac{d^2\delta}{dx^2} = -\frac{\xi x}{EI}$$

Apply integration on both sides

$$\delta = -\frac{\xi x^2}{6EI} + Ax + B \tag{19}$$

The constants A and B are required to be found out by utilizing the boundary condition, i.e. at x = l; d**δ**/dx = 0,

$$A = \frac{\xi l^2}{2EI} \tag{20}$$

At x= L; **δ**= 0,

$$\delta = -\frac{\xi l^3}{6EI} + Al + B$$

$$B = \frac{\xi l^3}{6EI} - Al$$

$$B = \frac{\xi l^3}{6EI} - \frac{\xi l^3}{2EI}$$

$$B = \frac{\xi l^3 - 3\xi l^3}{6EI} = -\frac{2\xi l^3}{6EI}$$

$$B = -\frac{\xi l^3}{3EI} \tag{21}$$

Substituting the values of A and B in equation 18, we will get

$$\delta = \frac{1}{EI}\left(-\frac{\xi x^2}{6EI} + \frac{\xi l^2 x}{2EI} - \frac{\xi l^2}{3EI}\right) \tag{22}$$

The slope as well as the deflection would be maximum at the free end hence putting x =0, then we can write,

$$\delta_{\max} = -\frac{\xi l^2}{3EI} \tag{23}$$

We know the relation between the spring constant and the displacement i.e.

$$\text{Spring constant} = K = \frac{\xi}{\delta_{\max}} = \frac{3EI}{l^2} \tag{24}$$

The above equation is the spring constant of a cantilever structure and the load is applied at the end. But in this paper we designed RF MEMS switch with clamped-clamped structure

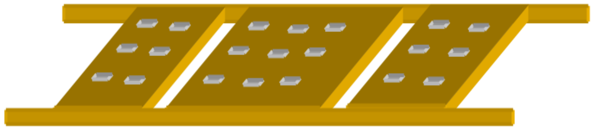

FIGURE 4. Schematic view of perforated clamped-clamped membrane.

shown in Figure 4. For that the spring are in parallel, so the equivalent spring constant is

$$K_{eq} = K_1 + K_2 + K_1 + K_2 \tag{25}$$

where,

$$K_{(1,2,3,4)} = \frac{Ewt^3}{l^3}$$

D. SIZE DEPENDENCY AND CRITICAL STRESS

According to the bernoulli-euler beam bending theory, the size of the membrane is also a key factor to decide the gradient elasticity (or) young's modulus and it can be expressed as [46]–[50]

$$E = \frac{FL}{A\ \Delta L} \tag{26}$$

Where, F force exerted on the membrane, L is the initial length, A is the area of cross section, and **ΔL** is the length of the amount by which the length of the object will change. From the equation 26, the elastic modulus of the membrane increases with increase in length and thereby decreases the pull in voltage and it is proven that the weight loss by the membrane with perforation is not more than 60% of the overall massThe perforated membrane will help to improve the performance of the RF MEMS switch.. To avoid the buckling effect in the fabrication of micro mechanical structures, better to do the stress analysis. The amount of compressive stress the membrane can withhold before buckling is which is a critical stress ($\boldsymbol{\sigma}_c$), for fixed-fixed beam it can be expresses as, [38], [39]

$$\sigma_c = \frac{\Pi^2 E t^2}{3l^2(1-\upsilon)} \tag{27}$$

E. RADIO FREQUENCY PARAMETERS

The perforated membrane eases the releasing process, and the perforated holes dimension is below 10 μm × 10μm then it won't be impact on the capacitance of the switch. The perforated area won't be more than 60% of overall area [51], [52].

The switch designed in this paper is a capacitive based, so the switching depend on the capacitance when the membrane is in up state and down state,i.e.,

$$C_{up} = \frac{\varepsilon_0 A_c}{g_1 + \frac{t_d}{\varepsilon_r}} + C_{ff} \tag{28}$$

$$C_{down} = \frac{\varepsilon_0 \varepsilon_r A_c}{t_d} \tag{29}$$

where, 'A_c' is the area between the membrane the CPW line, 't_d' is the dielectric thickness. The fringing field capacitance (C_{ff}) of the switch is 0.5 to 1.5 percentage of parallel plate capacitance. The characteristic impedance (Z_0) of the CPW transmission line can be defined as the circular integration of electric field over the length to the circular integration of magnetic field over the same length i.e.

$$Z_0 = \frac{V}{I} = \frac{\oint E}{\oint H} \tag{30}$$

The operation frequency and the characteristic impedance of the CPW transmission line is mainly depend on the width of center conductor (S) and the gap between the ground plane and the center conductor (G). In terms of S-parameters also we can find the characteristic impedance as

$$Z_0 = Z_I \sqrt{\frac{(1+S_{11})^2 - (S_{21})^2}{(1-S_{11})^2 - (S_{21})^2}} \tag{31}$$

The RF MEMS switch is designed using CPW transmission line. When the structure or membrane is in up state the input RF signal is allowed to the output port. The return losses (S_{11}) is used to measure how much input RF signal is reflected back, it can be written as

$$|S_{11}|^2 = \frac{\omega^2 C_{up}^2 Z_0^2}{4} \tag{32}$$

where, '$\boldsymbol{\omega}$' is the radio frequency, 'Z_0' characteristic impidance, 'Z_I' is the input impidance. The insertion losses (S_{21}) is used to measure how much input RF signal is reached to output port.

$$|S_{21}|^2 = \frac{1}{|S_{11}|^2}\left(\frac{C_{up}}{C_{down}}\right)^2 \tag{33}$$

When we apply electrostatic actuation voltage, the membrane get deforms and the switch won't allow the input RF signal to output port. The amount of isolation with respect to the radio frequency can be measured using isolation losses(S_{21}) i.e.

$$|S_{21}|^2 = \begin{cases} \dfrac{4}{\omega^2 C_{down}^2 Z_0^2} & \text{for } f \ll f_0 \\ \dfrac{4R_s^2}{Z_0^2} & for\ f \approx f_0 \\ \dfrac{4\omega^2 L^2}{Z_0^2} & for\ f \gg f_0 \end{cases} \tag{34}$$

III. DESIGN AND SIMULATION

The clampe-clamped micro mechanical membrane based RF MEMS switch is initially designed and simulated using finite element mehod tools like COMSOL and ANSYS HFSS. The mechanical behavior of the switch is analyzed using COMSOL tool and the microwave properties are analyzed using ANSYS HFSS tool. The switch membrane is actuated using two boottom electrodes by incorporating electrostatic actuation. The model RF MEMS switch structure is shown in the Figure 5, and switch dementions are listed in Table 1.

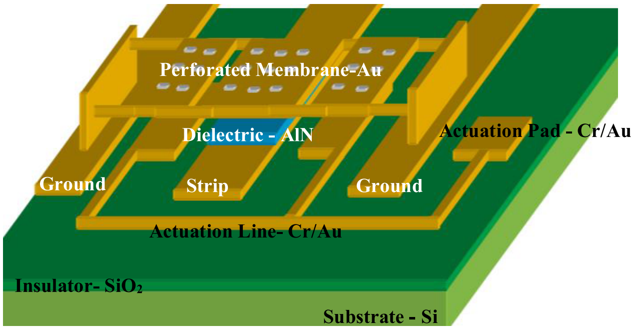

FIGURE 5. The structure of Clamped-Clamped membrane based RF Switch.

TABLE 1. Optimized shunt capacitive switch dimensions.

Parameter	Value (μm)
CPW (G-S-G)	90-60-90
Substrate width	400
Substrate length	500
Dioxide(insulator) thickness	1
Dielectric thickness	0.050
Dielectric constant(ε_r)	9.8
Bottom electrode width	60
Bottom electrode length	200
Gap between membrane and bottom electrode(g_2)	2
Overlap area under electrodes (A=2(W*w))	2(200*60)
Gap between dielectric and membrane (g_1)	1.8
Membrane thickness(t)	0.5
Membrane length (l)	430
Membrane width (w)	200
Area between membrane and CPW strip line (A_c)	200*60

Prior to fabrication we have analyzed the aspect ratio of the perforated membrane, i.e., the perforated area is not more than 60% overall area. The membrane perforation holes dimension is 5 μm × 5 μm. The critical stress of the membrane is 40 MPa. The perforation to the membrane impact on the quality factor of the switch. Low quality factor results low settling time. The switch designed in this paper offering a low quality factor of 0.68. The characteristic impedance of the switch is 54**Ω**, very close to source impedance. It is indicating that, this switch we can interface with an antenna with same input impedance.

The switch designed in this paper is a electrostatically actuated vertically deflective shunt capacitive RF MEMS switch. Therefore, the switch requiring an actuation voltage of 5.5V to get 1.8 μm displacement. The spring constant of the membrane is 4.585 N/m, resonant frequency is 8.91 KHz. The switch upstate capacitance is $C_{up} = 2.4$ fF, and the down state capacitance is 72.4 pF. The switch is offering and isolation of −72 dB at 21 GHz, and the overall in the frequency range 10 MHz to 40 GHz, the switch is offering −0.1 dB to −0.5 dB insertion losses.

IV. FABRICATION AND CHARACTERIZATION

The shunt capacitive RF MEMS switch is fabricated using surface micromachining, and the fabrication flow is shown in Figure 7. The switch is fabricated on 1145 μm × 540 μm size P-type Si <100> single side polished (SSP) substrate. A 1μm thickness, SiO_2 insulating layer is deposited using thermal oxidation at 1150°C. By using LOR and S1813 positive photoresist materials, CPW and actuation lines are patterned using liftoff process. Au is used for CPW and actuation lines. Cr[20 nm]/Au[200 nm]/Cr[20 nm] are deposited using DC sputtering with the target distance of 7.5 cm at room temperature.

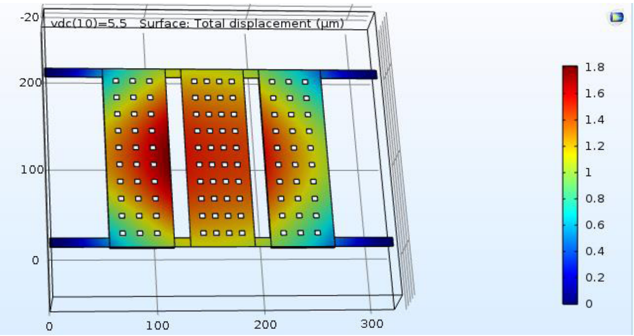

FIGURE 6. The Electrostatic actuation of shunt capacitive RF MEMS switch.

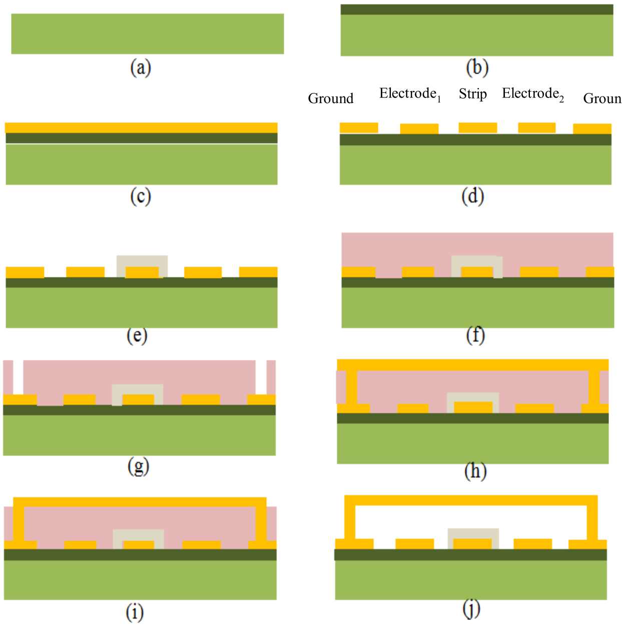

FIGURE 7. Fabrication flow, a) Si substrate, b) 1 μm Thickness SiO_2 insulator deposition using thermal oxidation, c) Cr[20 nm]/Au[200 nm] deposition using DC sputtering PVD process, d) Patterning of CPW and actuation lines using wet etching, e) Deposition and pattering of AlN of 50nm thickness using DC sputtering and RIE respectively, f) Deposition of sacrificial layer, g) Patterning of trenches, h)Deposition of membrane metal (Au), i) Patterning of membrane, j) Membrane release using wet process.

Here, Cr is used for better adhesion and to protect CPW and actuation lines. The switch fabricated in this paper, is a capacitive based switch. The dielectric material decides the insertion and isolation properties of the switch. Here, we have taken AlN as the dielectric material, and the 50 nm thickness of AlN material is deposited using DC sputtering. The AlN is patterned using reactive ion etching (RIE). In MEMS devices design, membrane releasing is difficult process. For this switch the membrane is released using wet process.

S1813 positive photo resist material is used as sacrificial layer. We coated a sacrificial layer of 1.8 μm using spin coater for 40 seconds with 2000 RPM. The membrane is Au material deposited using DC sputtering at 90 °C which helps the membrane to develop the strain. The membrane is patterned using wet etching with developer KI:I_2:H_2O in 4:01:40 ratio, after patterning of the membrane the switch is as shown in Figure 8.

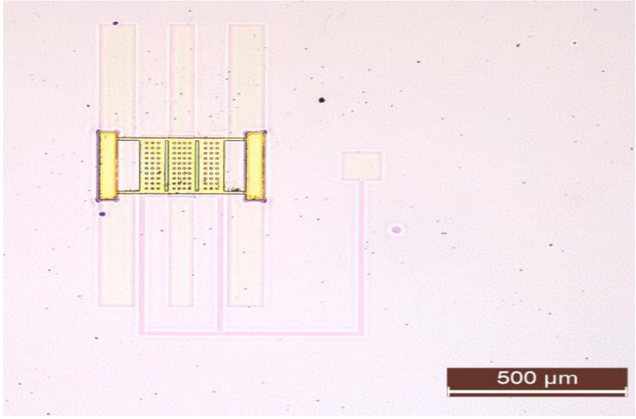

FIGURE 8. Membrane patterning on S1813 sacrificial layer.

However, the membrane is released using piranha cleaning for 5 minutes, and IPA for 5 minutes. To avoid the stiction problem in the switch we have done the critical point drying (CPD). We observed, the critical point values for the structure drying is pressure:1260 Psi, temperature:31 °C at this point liquid CO_2 convert into gaseous state. The final fabricated device is inspected with scanning electron microscope (SEM) results are shown in Figure 11 & 12.

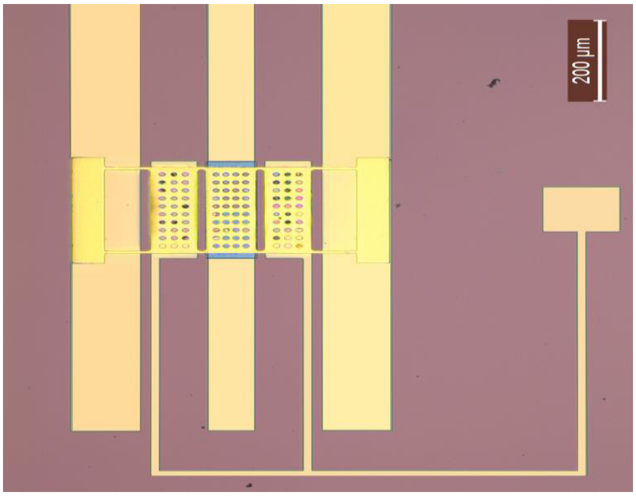

FIGURE 9. Membrane release using piranha, IPA and CPD:@ 200μm.

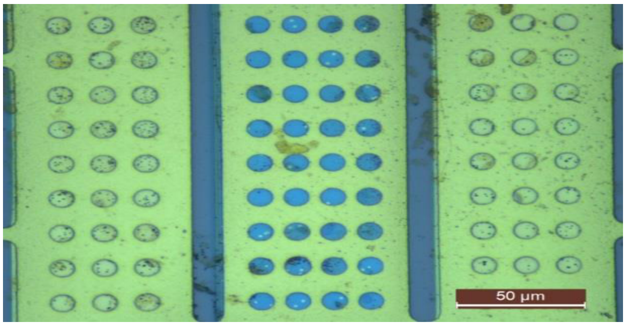

FIGURE 10. Membrane release using piranha, IPA and CPD:@ 50μm.

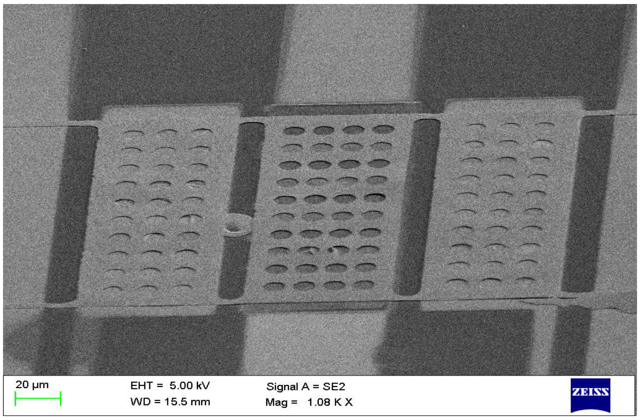

FIGURE 11. Membrane release using piranha, IPA and CPD:SEM view 1.

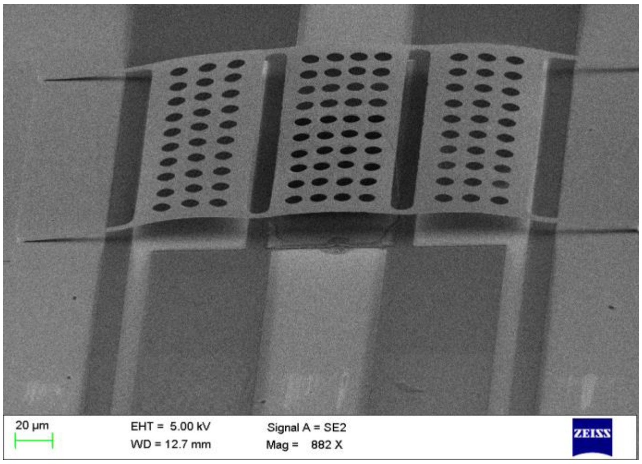

FIGURE 12. Membrane release using piranha, IPA and CPD:SEM view 2.

Mechanical characterization of the switch done by using micro system analyzer 500 (MSA 500). The electrical CV characteristics are measured using Agilent device analyzer B1500A with 5 MHz pulsed source. With this we have measured the upstate capacitance (C_{up}) and downstate capacitance(C_{down}) of the RF MEMS switch, the values are listed in the TABLE 2.

The designed and fabricated results like resonant frequency and the relation between supply voltage versus displacement as shown in Figure 14 & 15. Because of perfect execution of the fabrication steps like etching of membrane and the releasing of the membrane we are able to approximate the designed

TABLE 2. Present proposed work comparison with literature.

Shunt switches	Reference[16]	Reference[17]	Reference[18]	Proposed switch
Membrane material	Au	Au	Au	Au
Membrane dimensions [length, width, thickness]	530 µm, 214 µm, 1 µm	60 µm, 60 µm, 1 µm	170 µm, 100 µm, 2 µm	430 µm, 200 µm, 0.5 µm
Dielectric material	---	Si_3N_4	Si_xN_y	AlN
Dielectric dimensions [length, width, thickness]	92 µm, 70 µm, 0.2 µm	70 µm, 70 µm, 0.3 µm	100 µm, 50 µm, 0.3 µm	220 µm, 70 µm, 0.05 µm
Air gap(g_1)	---	3 µm	2 µm	1.8 µm
Upstate capacitance.	27 fF	9.8 fF	54 fF	2.4 fF
Downstate capacitance.	5.3 pF	0.83 pF	0.6 pF	72.4 pF
Insertion losses	-0.43 dB @35 GHz	-0.29 dB @35 GHz	-0.4 dB @35 GHz	-0.54 dB @27 GHz
Isolation losses	---	-20.5 dB @35 GHz	-38 dB @35 GHz	-72.4 dB @27 GHz
Actuation voltage	8 V	18.3 V	23 V	5.5 V
Switching time(t_s)	---	---	---	22 µs
Spring constant(K)	---	---	---	4.58 N/m
Rigid body mass(m)	---	---	---	104×10^{-12} Kg
Resonant frequency (f_r)	---	---	---	8.91 KHz


(a) (b) (c)

FIGURE 13. RF MEMS switch characterization setup, (a)DC probe station(Agilent B1500A), (b) RF probe station or vector network analyzer (Agilent E8361A), (c) Micro system analyzer.

and fabricated results. The switch radio frequency (RF) properties are analyzed using Agilent technologies E8361A RF probe station (or) vector network analyzer (VNA). The probe station is on wafer probing for the RF MEMS switches.

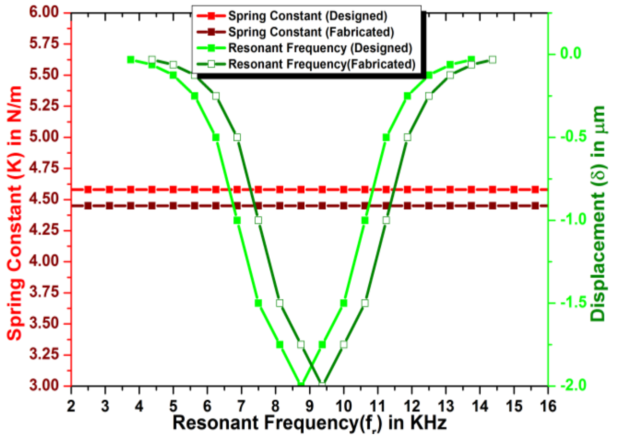

FIGURE 14. Resonant frequency (f_r) Vs Spring constant(K).

ACP65-A-GSG-200 probe is used for RF probing. Probe alignment is done using contact substrate and impedance standard substrate (ISS) is used for probe calibration.

In figure 15, we have related the applied supply voltage with membrane displacement of simulation using COMSOL FEM tool as well as measured after fabrication using micro system analyzer 500. The gap between the membrane and the bottom electrodes is 2 m. In both the cases, mean after design and fabrication results are very close with nominal difference. The microwave wave analysis is done over the frequency range 10 MHz to 40 GHz. The fabricated switch is offering −65 dB isolation at 27 GHz and the insertion losses are in the range −0.01 to −1.2 dB.

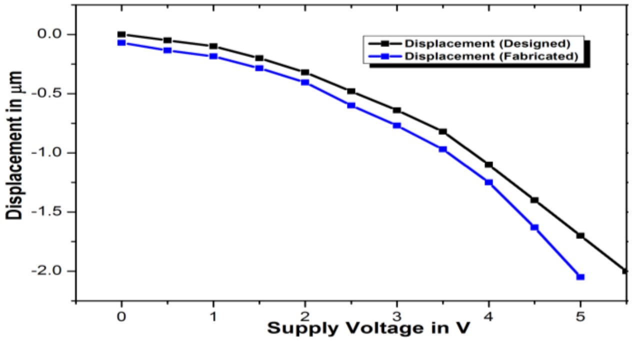

FIGURE 15. Supply voltage versus Displacement.

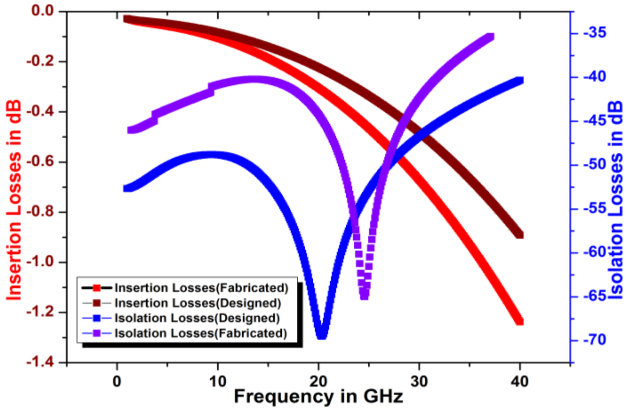

FIGURE 16. Insertion losses when membrane is in upstate, isolation losses when membrane is in downstate.

A. DIELECTRIC CHARGING CHARACTERIZATION

Dielectric charging behavior leads to the stiction problems in the MEMS switches. Dielectric charging is nothing but storage of unnecessary charge in the bottom dielectric thin film in the process of switch operation. If the charge deposited in the dielectric material is low, minimum pull in and pull up voltages are sufficient to deform and undeform the membrane. If the charge unnecessarily deposited in the dielectric material and in that, if the polarity of charge stored in the dielectric and opposite electrode is same then more pull in voltage require to deform the membrane, and if the polarity of charge stored in the dielectric is different to the opposite electrode charge then low pull in voltage required to deform the membrane but it require more pull up voltage to bring the membrane to the upstate position, sometime it may leads to permanent deformation of the membrane.

The dielectric charging behavior of the thin film may be characterized with CV curve pull-in voltage shift method. In this method manually the dielectric thin film is charged with other polarity charge when compared with opposite electrode charge polarity. That's why more pull in voltage means more charge is deposited in the dielectric thin film. With this we can relate pull in voltage with charge deposited in the dielectric material. Change in capacitance is measured using LCR meter. We have plotted the C-V graph before and after applying a stress at 65 V for 727 seconds. The schematic of dielectric charging characterization setup is shown in Figure 17. The charge is injected in to the dielectric thin film, by stressing it with the electric field on the order of 1 MV/cm. Because of this injected charge in the dielectric, which will impact the electric field present between the two electrodes in the process of electrostatic actuation. Because of this the amount of charge in the bottom and top electrode also changes, thereby influencing the electrostatic force. The net effect of the superimposed E-field is a shift of the C-V curve, which in turn affects the pull-in and pull-out voltages: $V_{pi} \Rightarrow V_{pi} + V_{shift}$ and $V_{po} \Rightarrow V_{po} + V_{shift}$. V_{shift} is proportional to the injected charge.

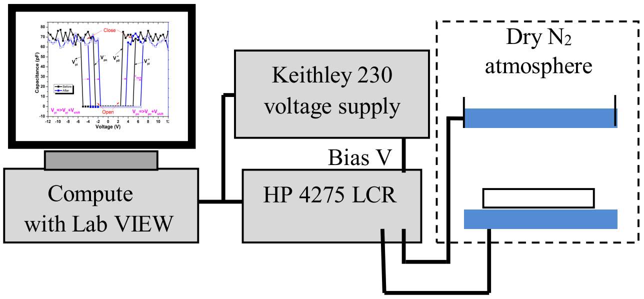

FIGURE 17. Schematic of dielectric charging characterization setup.

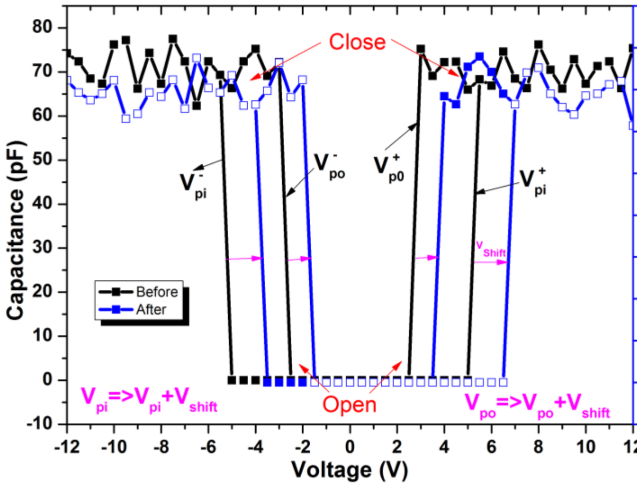

FIGURE 18. C-V curve before (black) and after (blue) applying pressure at 65 V for 727 seconds.

A large amount of injected charge can even lead to failure of the switch due to stiction of the top electrode to the dielectric. This happens when V_{po}^{-} becomes positive or when V_{po}^{+} become negative. The 50nm AlN dielectric material is offering a shift voltage of 1V, which is indicating that the dielectric charging effect is minimized.

V. CONCLUSIONS

In this paper, Clamped-Clamped micro mechanical structure based shunt capacitive switch is designed using FEM tools and fabricated using surface micro machining. The entire switch is fabricated on 1045 μm × 540 μm size Si wafer. Cr[20 nm]/Au[200 nm]/Cr[20 nm] metal layers are patterned for CPW and actuation lines. Here we are used Cr metal layer for better adhesion. A 50 nm thickness AlN is used as dielectric material with $\varepsilon_r = 9.8$. Au of 500 nm thickness is used as membrane material. S1813 is used as sacrificial layer and the membrane is released using wet process. We have also done the critical point drying (CPD) to avoid the dielectric charging based stiction problems. C-V curve of the dielectric material is drawn using HP 4275 LCR meter. By using C-V curve shifting method we characterized the dielectric charging behavior and we noticed that voltage shifting is low, and it is indicating that the dielectric charging effect is reduced. The fabricated of the perforated membrane reduces the pull in voltage i.e., 5.5V and eases the electrostatic actuation. We have used AlN as dielectric layer, therefore, it increases the isolation of the RF MEMS Switch. Finally, the overall switch is offering high isolation at 27 GHz frequency, hence, the Switch can use in K-band applications.

REFERENCES

[1] P. Chawla and R. Khanna, "Design, analysis and comparison of various MEMS switches for reconfigurable planar antenna," *Acta Polytechn. Hungarica*, vol. 11, no. 10, pp. 21–40, 2014.

[2] H. Rajagopalan, J. M. Kovitz, and Y. Rahmat-Samii, "MEMS reconfigurable optimized E-shaped patch antenna design for cognitive radio," *IEEE Trans. Antennas Propag.*, vol. 62, no. 3, pp. 1056–1064, Mar. 2014.

[3] T. J. Jung, I.-J. Hyeon, C.-W. Baek, and S. Lim, "Circular/linear polarization reconfigurable antenna on simplified RF-MEMS packaging platform in K-band," *IEEE Trans. Antennas Propag.*, vol. 60, no. 11, pp. 5039–5045, Nov. 2012.

[4] A. Zohur, H. Mopidevi, D. Rodrigo, M. Unlu, L. Jofre, and B. A. Cetiner, "RF MEMS reconfigurable two-band antenna," *IEEE Antennas Wireless Propag. Lett.*, vol. 12, pp. 72–75, 2013.

[5] S. Zhang, W. Su, M. Zaghloul, and B. Thibeault, "Wideband CMOS compatible capacitive MEMS switch for RF applications," *IEEE Microw. Wireless Compon. Lett.*, vol. 18, no. 9, pp. 599–601, Sep. 2008.

[6] S. Molaei and B. Z. Ganji, "Design and simulation of a novel RF MEMS shunt capacitive switch with low actuation voltage and high isolation," *Microsyst. Technol.*, vol. 23, no. 6, pp. 1907–1912, 2016, doi: 10.1007/s00542-016-2923-2.

[7] K. Guha, N. M. Laskar, H. J. Gogoi, A. K. Borah, K. L. Baishnab, and S. Baishya, "Novel analytical model for optimizing the pull-in voltage in a flexured MEMS switch incorporating beam perforation effect," *Solid-State Electron.*, vol. 137, pp. 85–94, Nov. 2017.

[8] H.-H. Yang, C.-H. Han, S.-J. Choi, D.-H. Choi, and J.-B. Yoon, "Signal power-insensitive analog MEMS tunable capacitor by immobilizing the movable plates," *J. Microelectromech. Syst.*, vol. 24, no. 5, pp. 1545–1556, 2015, doi: 10.1109/JMEMS.2015.2420121.

[9] D. Peroulis, S. P. Pacheco, K. Sarabandi, and L. P. B. Katehi, "Electromechanical considerations in developing low-voltage RF MEMS switches," *IEEE Trans. Microw. Theory Techn.*, vol. 51, no. 1, pp. 259–270, Jan. 2003.

[10] L. Dussopt and G. M. Rebeiz, "Intermodulation distortion and power handling in RF MEMS switches, varactors, and tunable filters," *IEEE Trans. Microw. Theory Techn.*, vol. 51, no. 4, pp. 1247–1256, Apr. 2003.

[11] Y. S. Hijazi, Y. A. Vlasov, and G. L. Larkins, "Design of a superconducting MEM shunt switch for RF applications," *IEEE Trans. Appl. Supercond.*, vol. 13, no. 2, pp. 696–699, Jun. 2003.

[12] A. T. Alastalo, T. Mattila, and H. Seppä, "Analysis of a MEMS transmission line," *IEEE Trans. Microw. Theory Techn.*, vol. 51, no. 8, pp. 1977–1981, Aug. 2003.

[13] D. Saias *et al.*, "An above IC MEMS RF switch," *IEEE J. Solid-State Circuits*, vol. 38, no. 12, pp. 2318–2324, Dec. 2003.

[14] M. A. Philippine, H. Zareie, O. Sigmund, G. M. Rebeiz, and T. W. Kenny, "Experimental validation of topology optimization for RF MEMS capacitive switch design," *J. Microelectromech. Syst.*, vol. 22, no. 6, pp. 1296–1309, Dec. 2013.

[15] M. A. Philippine, O. Sigmund, G. M. Rebeiz, and T. W. Kenny, "Topology optimization of stressed capacitive RF MEMS switches," *J. Microelectromech. Syst.*, vol. 22, no. 1, pp. 206–215, Feb. 2013.

[16] U. Sharma *et al.*, "Fabrication process induced changes in scattering parameters of meander type RFMEMS shunt switch," *Microsyst. Technol.*, vol. 23, no. 12, pp. 5561–5570, 2017, doi: 10.1007/s00542-017-3314-z.

[17] M. Li, J. Zhao, Z. You, and G. Zhao, "Design and fabrication of a low insertion loss capacitive RF MEMS switch with novel micro-structures for actuation," *Solid-State Electron.*, vol. 127, pp. 32–37, Jan. 2016, doi: 10.1016/j.sse.2016.10.004.

[18] K. Demirel, E. Yazgan, Ş. Demir, and T. Akın, "A new temperature-tolerant RF MEMS switch structure design and fabrication for ka-band applications," *J. Microelectromech. Syst.*, vol. 25, no. 1, pp. 60–68, Feb. 2016.

[19] S. Fouladi and R. R. Mansour, "Capacitive RF MEMS switches fabricated in standard 0.35-μm CMOS technology," *IEEE Trans. Microw. Theory Techn.*, vol. 58, no. 2, pp. 478–486, Feb. 2010.

[20] R. Ramadoss, S. Lee, Y. C. Lee, V. M. Bright, and K. C. Gupta, "Fabrication, assembly, and testing of RF MEMS capacitive switches using flexible printed circuit technology," *IEEE Trans. Adv. Packag.*, vol. 26, no. 3, pp. 248–254, Aug. 2003.

[21] Y. S. Hijazi, D. Hanna, D. Fairweather, Y. A. Vlasov, and G. L. Larkins, "Fabrication of a superconducting MEM shunt switch for RF applications," *IEEE Trans. Appl. Supercond.*, vol. 13, no. 2, pp. 700–703, Jun. 2003.

[22] V. Mulloni, B. Margesin, P. Farinelli, R. Marcelli, A. Lucibello, and G. De Angelis, "Cycling reliability of RF-MEMS switches with gold-platinum multilayers as contact material," *Microsyst. Technol.*, vol. 23, no. 9, pp. 3843–3850, 2015, doi: 10.1007/s00542-015-2782-2.

[23] A. Persano, A. Cola, G. De Angelis, A. Taurino, P. Siciliano, and F. Quaranta, "Capacitive RF MEMS switches with tantalum-based materials," *J. Microelectromech. Syst.*, vol. 20, no. 2, pp. 365–370, Apr. 2011.

[24] J. B. Rizk and G. M. Rebeiz, "W-band CPW RF MEMS circuits on quartz substrates," *IEEE Trans. Microw. Theory Techn.*, vol. 51, no. 7, pp. 1857–1862, Jul. 2003.

[25] L. L. Mercado, T.-Y. T. Lee, S.-M. Kuo, V. Hause, and C. Amrine, "Thermal solutions for discrete and wafer-level RF MEMS switch packages," *IEEE Trans. Adv. Packag.*, vol. 26, no. 3, pp. 318–326, Aug. 2003.

[26] D. Mardivirin, A. Pothier, A. Crunteanu, B. Vialle, and P. Blondy, "Charging in dielectricless capacitive RF-MEMS switches," *IEEE Trans. Microw. Theory Techn.*, vol. 57, no. 1, pp. 231–236, Jan. 2009.

[27] X. Yuan, Z. Peng, J. C. M. Hwang, D. Forehand, and C. L. Goldsmith, "Acceleration of dielectric charging in RF MEMS capacitive switches," *IEEE Trans. Device Mater. Rel.*, vol. 6, no. 4, pp. 556–563, Dec. 2006.

[28] M. Koutsoureli, L. Michalas, and G. Papaioannou, "The effect of temperature on dielectric charging of capacitive MEMS," in *Proc. IEEE Int. Rel. Symp.*, Apr. 2011, pp. 290–296.

[29] U. Zaghloul, F. Coccetti, G. J. Papaioannou, P. Pons, and R. Plana, "A novel low cost failure analysis technique for dielectric charging phenomenon in electrostatically actuated MEMS devices," in *Proc. IEEE Int. Rel. Symp.*, May 2010, pp. 237–245.

[30] J. Wibbeler, G. Pfeifer, and M. Hietschold, "Parasitic charging of dielectric surfaces in capacitive microelectromechanical systems (MEMS)," *Sens. Actuators A, Phys.*, vol. 71, pp. 74–80, Nov. 1998.

[31] R. W. Herfst, H. G. A. Huizing, P. G. Steeneken, and J. Schmitz, "Characterization of dielectric charging in RF MEMS capacitive switches," in *Proc. IEEE Int. Conf. Microelectron. Test Struct.*, Mar. 2006, pp. 133–136.

[32] M. Koutsoureli, L. Michalas, and G. Papaioannou, "Charge collection mechanism in MEMS capacitive switches," in *Proc. IEEE Int. Rel. Symp.*, Apr. 2012, pp. ME.2.1–ME.2.5.

[33] S. Agarwal, R. Kashyap, K. Guha, and S. Baishya, "Modeling and analysis of capacitance in consideration of the deformation in RF MEMS shunt switch," *Super Lattices Microstruct.*, vol. 101, pp. 567–574, Jan. 2016, doi: 10.1016/j.spmi.2016.10.022.

[34] G. M. Rebeiz and J. B. Muldavin, "RF MEMS switches and switch circuits," *IEEE Microw. Mag.*, vol. 2, no. 4, pp. 59–71, Dec. 2001.

[35] K. Guha, M. Kumar, A. Parmar, and S. Baishya, "Performance analysis of RF MEMS capacitive switch with non uniform meandering technique," *Microsyst. Technol.*, vol. 22, no. 11, pp. 2633–2640, 2016.

[36] R. Barretta, F. M. de Sciarra, and M. Diaco, "Small-scale effects in nanorods," *Acta Mech.*, vol. 225, no. 7, pp. 1945–1953, Jul. 2014, doi: 10.1007/s00707-013-1034-8.

[37] R. Barretta and F. M. de Sciarra, "Analogies between nonlocal and local Bernoulli–Euler nanobeams," *Arch. Appl. Mech.*, vol. 5, no. 1, pp. 89–99, Aug. 2014, doi: 10.1007/s00419-014-0901-7.

[38] R. Barretta, L. Feo, R. Luciano, and F. M. de Sciarra, "Application of an enhanced version of the Eringen differential model to nanotechnology," *Compos. B, Eng.*, vol. 96, pp. 274–280, Jul. 2016, doi: 10.1016/j.compositesb.2016.04.023.

[39] R. Barretta, M. Brčić, M. Čanađija, R. Luciano, and F. M. de Sciarra, "Application of gradient elasticity to armchair carbon nanotubes: Size effects and constitutive parameters assessment," *Eur. J. Mech. A, Solids*, vol. 65, pp. 1–13, Sep./Oct. 2017, doi: 10.1016/j.euromechsol.2017.03.002.

[40] R. Barretta and F. M. de Sciarra, "Constitutive boundary conditions for nonlocal strain gradient elastic nano-beams," *Int. J. Eng. Sci.*, vol. 130, pp. 187–198, Sep. 2018, doi: 10.1016/j.ijengsci.2018.05.009.

[41] S. A. Faghidian, "Integro-differential nonlocal theory of elasticity," *Int. J. Eng. Sci.*, vol. 129, pp. 96–110, Aug. 2018, doi: 10.1016/j.ijengsci.2018.04.007.

[42] S. A. Faghidian, "Reissner stationary variational principle for nonlocal strain gradient theory of elasticity," *Eur. J. Mech. A, Solids*, vol. 70, pp. 115–126, Feb. 2018, doi: 10.1016/j.euromechsol.2018.02.009.

[43] D. Abbondanza *et al.*, "Linear dynamic response of nanobeams accounting for higher gradient effects," *J. Appl. Comput. Mech.*, vol. 2, no. 2, pp. 54–64, 2016.

[44] M. Zarei, G. R. Faghani, M. Ghalami, and G. H. Rahimi, "Buckling and vibration analysis of tapered circular nano plate," *J. Appl. Comput. Mech.*, vol. 4, no. 1, pp. 40–54, 2018, doi: 10.22055/JACM.2017.22176.1127.

[45] D. P. Zhang, Y. Lei, and Z. B. Shen, "Semi-analytical solution for vibration of nonlocal piezoelectric kirchhoff plates resting on viscoelastic foundation," *J. Appl. Comput. Mech.*, vol. 4, no. 3, pp. 202–215, 2017, doi: 10.22055/jacm.2017.23096.1149.

[46] H. M. Sedighi, A. Koochi, and M. Abadyan, "Modeling the size dependent static and dynamic pull-in instability of cantilever nanoactuator based on strain gradient theory," *Int. J. Appl. Mech.*, vol. 6, no. 5, p. 1450055, 2014, doi: 10.1142/S1758825114500550.

[47] H. M. Sedighi, F. Daneshmand, and M. Abadyan, "Modeling the effects of material properties on the pull-in instability of nonlocal functionally graded nano-actuators," *J. Appl. Math. Mech./Zeitschrift fÃijr Angewandte Math. Mech.*, vol. 96, no. 3, pp. 385–400, 2016, doi: 10.1002/.zamm.201400160.

[48] A. Koochi, H. M. Sedighi, and M. Abadyan, "Modeling the size dependent static and dynamic pull-in instability of cantilever nanoactuator based on strain gradient theory," *Latin Amer. J. Solids Struct.*, vol. 11, no. 10, pp. 1806–1829, 2014.

[49] R. Barretta, M. Čanađija, L. Feo, R. Luciano, F. M. de Sciarra, and R. Penna, "Exact solutions of inflected functionally graded nano-beams in integral elasticity," *Compos. B, Eng.*, vol. 142, pp. 273–286, Jun. 2018, doi: 10.1016/j.compositesb.2017.12.022.

[50] Ç. Demir, K. Mercan, H. M. Numanoglu, and Ö. Civalek, "Bending response of nanobeams resting on elastic foundation," *J. Appl. Comput. Mech.*, vol. 4, no. 2, pp. 105–114, 2018, doi: 10.22055/JACM.2017.22594.1137.

[51] B. D. Jensen, K. Saitou, J. L. Volakis, and K. Kurabayashi, "Fully integrated electrothermal multidomain modeling of RF MEMS switches," *IEEE Microw. Wireless Compon. Lett.*, vol. 13, no. 9, pp. 364–366, Sep. 2003.

[52] M. Barbato, V. Giliberto, A. Cester, and G. Meneghesso, "A combined mechanical and electrical characterization procedure for investigating the dynamic behavior of RF-MEMS switches," *IEEE Trans. Device Mater. Rel.*, vol. 14, no. 1, pp. 13–20, Mar. 2014.

K. SRINIVASA RAO (M'17) was born in Andhra Pradesh, India. He received the master's and Ph.D. degrees from Central University. He is currently a Professor and the Head of the Microelectronics Research Group, Department of Electronics and Communication Engineering, Koneru Lakshmaiah Education Foundation (Deemed to be University), Guntur, India. He is working on the MEMS project worth of 40 lakhs funded by SERB, Government of India. He has published more than 94 international research publications and presented more than 45 conference technical papers around the world. His current research areas are MEMS-based reconfigurable antenna's actuators, bio-MEMS, RF MEMS switches, and RF MEMS filters. He is an Technical Society Member of IETE, ISTE, and IEEE Bodies. He received the Young Scientist Award from the Department of Science and Technology, Government of India, in 2011, the UGC Major Research Project in 2012, and the Early Career Research Award from SERB, Government of India, in 2016. He is collaborated research work with NIT's, Central Universities, IIT's, and so on. Three Ph.D. Scholars has been Awarded under his Guidelines and seven Ph.D. Scholars are currently working with him.

LAKSHMI NARAYANA THALLURI (M'16) was born in Ponnur, Andhra Pradesh, India. He received the B.Tech. degree in electronics and communication engineering from Jawaharlal Nehru Technological University, Kakinada, in 2009, and the M.Tech. degree in electronics & communication engineering (VLSI) from K L University in 2012. He is currently pursuing the part-time Ph.D. degree with the Koneru Lakshmaiah Education Foundation (Deemed to be University), Guntur, India. He is also an Assistant Professor with the Department of Electronics & Communication Engineering, Andhra Loyola Institute of Engineering Technology, Vijayawada, India. His current research area is RF MEMS switches and Internet of Things. He is a member of IE and IACSIT.

KOUSHIK GUHA received the B.Tech. degree in electronics and communication engineering from Techno India, Salt Lake, Kolkata, in 2005, under the West Bengal University of Technology, India, the M.Tech. degree in electronics and communication engineering (RF and microwaves) from Burdwan University, India, in 2007, and the Ph.D. degree from the National Institute of Technology (NIT) at Silchar in 2016, with a focus on design and modeling of RF MEMS shunt switch. From 2007 to 2010, he was a Lecturer with the Department of Electronics and Communication Engineering, Haldia Institute of Technology, India. He has been an Assistant Professor with the Department of Electronics and Communication Engineering, NIT Silchar, since 2010. From 2012 to 2014, he was a Visiting Faculty Member with NIT Mizoram. He is a member of IETE.

K. GIRIJA SRAVANI was born in Andhra Pradesh, India. She received the bachelor's degree in electronics and communication engineering, and the master's degree in VLSI & embedded systems from Jawaharlal Nehru Technological University, Kakinada. She is currently pursuing the Ph.D. degree in RFMEMS Research domain with the National Institute of Technology, Silchar. She is also an Assistant Professor with the Department of Electronics & Communication Engineering, K L University, Guntur, India. She is currently working on MEMS Project worth of 40 Lakhs funded by SERB, Government of India. She has published over 25 International research publications and presented over five conference technical papers around the world. Her current research areas are MEMS and RF MEMS.